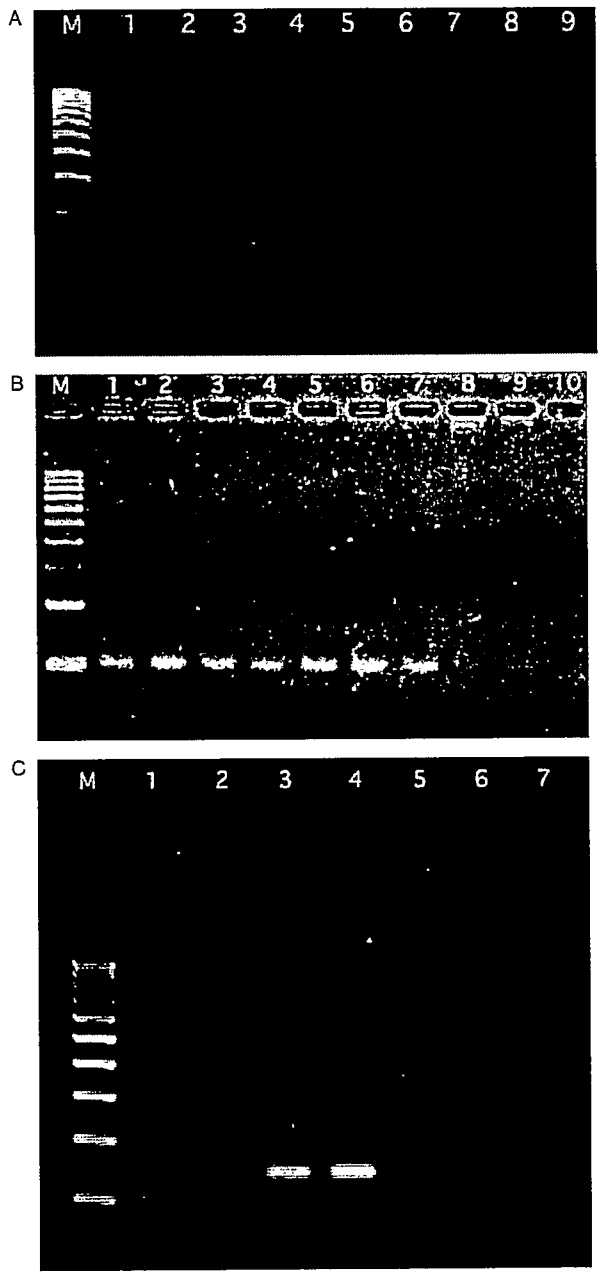

FIGURE 3. Results of mutation-specific PCR. A, DelE746-A750-specific PCR for tumor samples. Lane 1: H1650; lanes 2 and 3: samples with deletion of nucleotides 2481-2495 (19del-type1); lanes 4 and 5: samples with deletion of nucleotides 2482-2496 (19del-type2); lanes 6 to 9: samples without deletion. M: 100-bp molecular marker. B, L858R-specific PCR for tumor samples. Lane 1: H1975; lanes 2 to 7: samples with mutation 2819(T > G); lanes 8 to 10: samples without mutation. C, "Dual-specific PCR" for tumor samples. Lanes 1 and 2: samples with L858R mutation, 104-bp bands are visible; lanes 3 and 4: samples with delE746-A750, 133-bp bands are visible; lanes 5 to 7: samples without mutation or deletion.

attenuated specificity of 19ASD1. Samples showing a positive band for delE746-A750-specific PCR exactly matched those shown to include either 19del-type1 or 19del-type2 delE746-A750 on sequence analysis. No positive bands were detected in samples without a deletion in exon 19 or in samples with types of deletion other than delE746-A750. These results suggest that this primer set can be used for detecting both 19del-type1 and 19del-type2.

L858R-specific PCR

L858R-specific PCR was also performed using primers 21SM1 and 21AS4 for cell line H1975, revealing a band with the expected size of 104 bp (Fig. 3). No positive bands were detected for the 50 normal samples.

In the analysis of tumor samples, 14 of 62 samples yielded positive bands for L858R-specific PCR (Fig. 3). Interestingly, although 11 of these 14 samples had already been judged as having the L858R mutation by sequence analysis, the remaining 3 samples detected as positive by L858R-specific PCR had not been judged as mutated on direct sequence analysis in the first investigation. Close inspection after L858R-specific PCR revealed that these 3 samples actually harbored very low mutated signals at nucleotide 2819 that were difficult to distinguish from background noise (Fig. 4). These 3 samples were considered to contain a low percentage of DNA with the L858R mutation. The remaining 48 samples that were negative on L858R-specific PCR did not show any level of mutated signal on closer inspection, and were regarded as genuinely negative for L858R.

Mutation-specific PCR Detecting Both Types of Mutation

Dual-specific PCR was performed for all samples by mixing 2 sets of primers in a single reaction mix. Samples with delE746-A750 demonstrated a 133-bp band and samples with L858R showed a 104-bp band, indicating that the 2 sets of primers did not hamper each other in detecting specific mutations in the reaction mix (Fig. 3). Samples judged as positive in this dual-specific PCR exactly matched those judged as positive on single delE746-A750-specific or L858R-specific PCR. No false-positive results were obtained from samples without these mutations.

DNA Mixture Analysis

Mutation-specific PCR was performed for DNA mixtures containing various proportions of mutant DNA. As the proportion of mutant DNA decreased, the intensity of the band generated by PCR became increasingly faint (Fig. 5). In delE746-A750-specific PCR, a DNA mixture containing 2.5% mutant alleles, which was assumed to be derived from a sample containing 5% mutant cells, could be detected as positive. In L858R-specific PCR, a DNA mixture containing as little as 0.25% mutant alleles displayed a positive band. On the basis of these results, we concluded that delE746-A750 and L858R were detectable by mutation-specific PCR

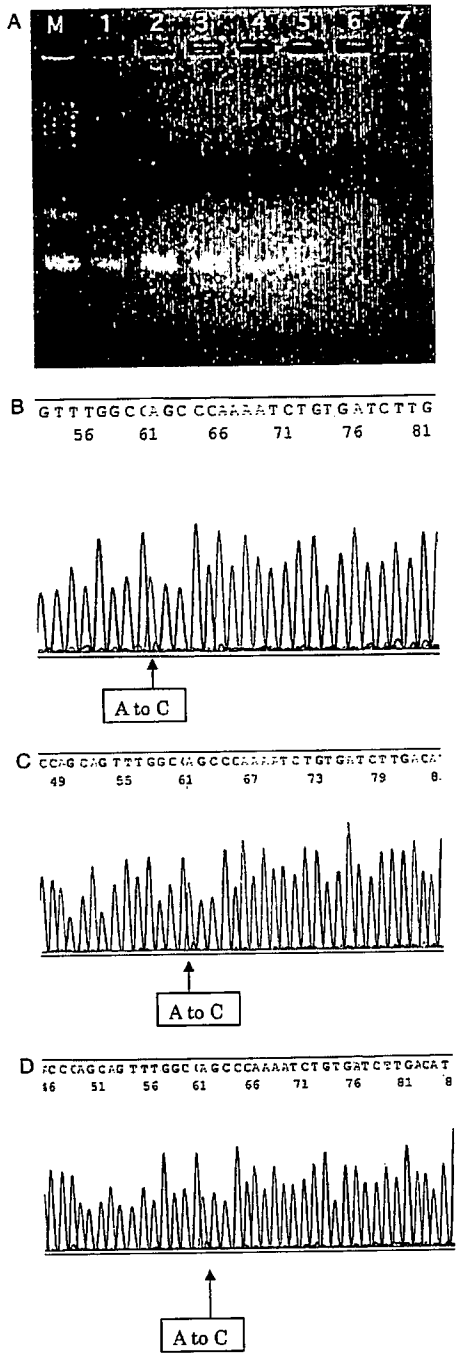

FIGURE 4. Cases with L858R mutation barely detectable by sequence analysis. A, Results of L858R-specific PCR for these samples. A band with expected size is clearly detected (lanes 1 to 3). Lane 4: positive controls; lanes 5 to 7: negative controls. B to D, Results of sequence analysis in the reverse direction. The A to C mutation at nucleotide 2819 is faintly visible, but is not readily distinguishable from background noise around nearby sequences.

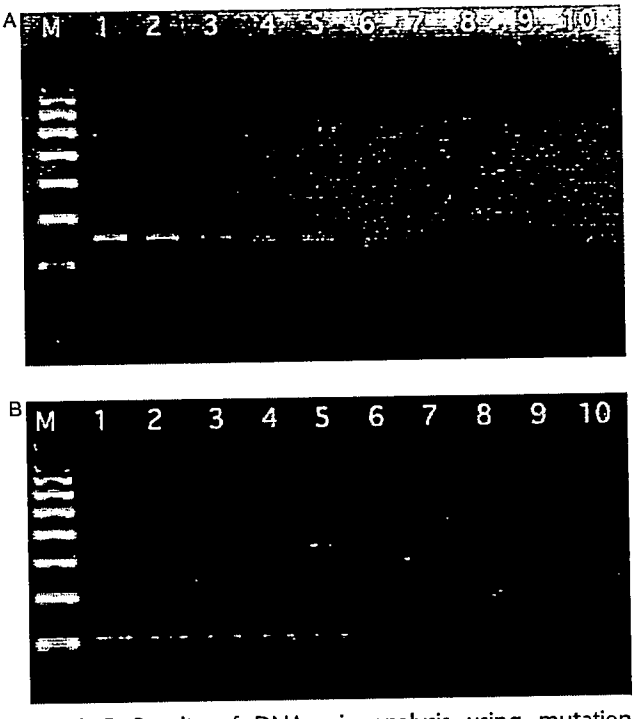

FIGURE 5. Results of DNA mix analysis using mutation-specific PCR. A, DNA mixture analysis of delE746-A750-specific PCR. Lanes 1 to 10: PCR for various proportions of deleted DNA from H1650. Lanes represent PCR product from DNA containing 50%, 25%, 10%, 5%, 2.5%, 1%, 0.5%, 0.25%, 0.1%, and 0% mutant alleles, respectively. A positive band is detected in samples with as little as 2.5% deleted DNA. M: 100-bp molecular marker. B, DNA mixture analysis of L858R-specific PCR. Lanes 1 to 10: PCR for various proportions of deleted DNA from H1975. Lanes represent PCR product from DNA containing 50%, 25%, 10%, 5%, 2.5%, 1%, 0.5%, 0.25%, 0.1%, and 0% mutant alleles, respectively. A positive band is detected in samples with as little as 0.25% mutant DNA.

methods even if tumor samples included up to 95% or 99.5% of contaminating tissue, respectively.

DISCUSSION

Newly developed TKIs are attractive as anticancer drugs. After the successful clinical introduction of imatinib for chronic myelogenous leukemia,[16] gefitinib was developed as a promising TKI against lung cancer. However, gefitinib is currently available for clinical use only in Japan and the United States, and recipients are limited by guidelines in these countries because of the frequent development of life-threatening interstitial pneumonia.[17–19] Given this serious adverse effect, protocols for selecting patients who will benefit most from gefitinib therapy are eagerly awaited. One potential way for predicting the consequences of gefitinib therapy would be the detection of mutations within the *EGFR* gene, because the presence of *EGFR* mutations in tumors

reportedly displays a strong correlation with the clinical efficacy of gefitinib.[4–6] Simple, sensitive, and reliable methods to detect *EGFR* mutations in lung tumor samples are therefore needed to achieve optimal use of this drug in clinical settings.

Sequence analysis of tumor DNA is the most widely applied method for detecting *EGFR* mutations in lung cancer, and is considered the most direct and reliable approach. However, the method has several disadvantages, the most notable being difficulties in detecting mutations in the presence of contaminated normal tissues in tumor samples. Specimens of lung tumor usually contain substantial proportions of normal cells, such as those from fibrous tissue and peripheral blood. Previous reports have noted that a positive result from direct sequencing requires $\geq 30\%$ of mutant DNA in the sample.[20] Considering that most *EGFR* mutations in lung cancer are heterozygous, the presence of 50% normal cells might easily conceal the mutation from detection. In addition, sequence analysis is relatively expensive and time consuming. Direct sequencing requires amplification with Taq polymerase (2 to 3 h), purification ($\sim$1 h), second DNA polymerization ($\sim$2 h), and, finally, sequence detection ($\sim$1 h). To confirm the mutation, sequencing from sense and anti-sense directions is required, doubling this time requirement. The handling involved in these multiple steps may increase the rate of failures because of factors such as high background noise. Direct sequencing may therefore not be ideal in terms of sensitivity or simplicity.

Single-strand conformation polymorphism analysis is an easier and less expensive method for detecting small genetic mutations.[20,21] The technique also offers superior sensitivity, allowing the detection of mutations in samples containing as little as 10% mutant DNA. However, this method is not yet clinically familiar, and few laboratories can perform this analysis. Mutation-specific, real-time PCR has also been reported to offer superior sensitivity to sequencing, but requires special instruments and precise techniques that are unavailable in most clinical institutes.[22] Most recently, Pan et al[23] reported a rapid PCR-based method to detect *EGFR* mutations. This approach is superior to direct sequencing in the rapid detection of mutations within exons 19 and 21, and the technique is relatively simple and widely available. However, the method remains rather complicated, because different techniques are used between exons 19 and 21 for the detection of mutations, and a sequencing machine is needed.

In contrast, our mutation-specific PCR method allows quick and accurate detection of the most important *EGFR* mutations in lung cancer samples. In this study, the new method successfully detected all specific mutations (delE746-A750 and L858R) revealed by sequence analysis, and did not generate any positive bands for 50 normal samples. As revealed by DNA mixture analysis, mutation-specific PCR could provide positive results for as little as 2.5% (delE746-A750) or 0.25% (L858R) of mutant DNA mixed in normal DNA. Although the proportion of mutated DNA in a cell line may be slightly more than 50% and the sensitivity of mutation-specific PCR slightly worse, superiority to the sensitivity of direct sequencing remains. This method thus seems extremely accurate and sensitive for detecting specific mutations. In some cases, this method was actually superior to direct sequencing, clearly identifying 3 L858R mutations that were not initially detected on direct sequencing. At the very least, this method would seem useful for confirming the presence of specific mutations in cases where the result of sequence analysis is ambiguous because of high levels of background noise.

Furthermore, we attempted to apply dual-specific PCR to formalin-fixed, paraffin-embedded tumor tissues, and successfully detected delE746-A750 and L858R mutations (data not shown). In contrast, no positive bands were detected when identical methods were applied to paraffin-embedded normal tissues. This means that the present method can be applied to large numbers of stock samples previously stored as paraffin-embedded materials, even when these samples are unavailable as frozen materials. This will enormously broaden the range of applications for this method.

The present method is also cost and labor efficient. After DNA extraction, only 1 cycle of amplification and less than 1 hour of electrophoresis per 10 to 15 samples is needed to obtain a result. DelE746-A750-specific and L858R-specific PCR can even be performed concurrently in the same reaction, as demonstrated by dual-specific PCR analysis. The presence of specific mutations can thus be detected within 1 day of starting DNA extraction. The running cost of PCR and electrophoresis is considerably lower than that of sequence analysis.

Technical simplicity and the easy availability of the required equipment are also highly advantageous. PCR can readily be performed in laboratories equipped with PCR and electrophoresis systems together with some other minor instruments. The cost of the requisite equipment is again much lower than that of a sequence analyzer. PCR can therefore be performed even in clinical laboratories, and is not limited to research laboratories. In recent years, a growing number of clinical laboratories have been equipped with PCR systems for other clinical applications.

The most evident limitation of this technique is that not all the *EGFR* mutations that lung cancer may harbor can be detected. Although > 90% of mutations cluster in exons 19 and 21, infrequent mutations have been reported in exons 18 and 20, and mutations on exons 19 and 21 other than those examined here have also been reported.[5–11] Table 3 summarizes the *EGFR* mutations in NSCLC that have been described in major reports.[4–11,13,24] About 60% of exon 19 deletion mutations are delE746-A750 mutations, whereas around 90% of exon 21 mutations are L858R mutations. Overall, our mutation-specific PCR would detect about 70% of reported cases involving mutations. Alternative methods are thus needed to detect the remaining 30% of *EGFR* mutations. We actually attempted to generate PCR

primers capable of detecting 18-bp deletions within exon 19, and these successfully detected the specific deletion by PCR under similar conditions (data not shown). However, inclusion of numerous types of PCR would in turn reduce the convenience of this mutation-specific PCR test. Decisions should be made depending on the clinical situation as to whether additional tests to detect other types of mutation should be performed, taking into account factors such as clinical benefit, availability, complexity, accuracy, and cost.

Another possible application of this method would be to detect the scattering of tumor cells within lungs or minimal metastasis beyond the lungs in patients with these specific mutations. As NSCLC does not display specific tumor markers, detecting tumor scattering or metastases in tissues with $< 10\%$ of tumor cells is difficult. L858R-specific PCR can detect as little as 0.5% of tumor cells, and so may be useful for detecting minimal invasion of tumor cells in lymph nodes and other tissues. Further studies combined with precise histological investigation are necessary to elucidate the efficacy of this technique in detecting tumor scattering or minimal metastasis.

In conclusion, we have developed a simple and sensitive method to detect major mutations of the *EGFR* gene in lung cancer samples. Sensitivity, specificity, cost, and simplicity of the procedure are satisfactory for genetic testing of lung cancer patients at the clinical laboratory level. This method will provideimportant information regarding the pathophysiology of lung cancer, in addition to facilitating medical decisions on treatment using TKI for patients. Detection of minimal metastasis in lung cancer patients with specific *EGFR* mutations may also be possible.

ACKNOWLEDGMENTS

The authors express their gratitude to Dr Sakamoto and his colleagues at the Department of Pathology of Kyorin University for their professional histological investigations, as well as for providing the authors with paraffin-embedded tissue samples.

REFERENCES

1. Jemal A, Tiwari RC, Murray T, et al. American Cancer Society. Cancer statistics, 2004. *CA Cancer J Clin.* 2004;54:8–29.
2. Parkin DM, Bray FI, Devesa SS. Cancer burden in the year 2000. The global picture. *Eur J Cancer.* 2001;37(Suppl 8):4–66.
3. Schiller JH, Harrington D, Belani CP, et al. Eastern Cooperative Oncology Group. Comparison of four chemotherapy regimens for advanced non-small-cell lung cancer. *N Engl J Med.* 2002;346:92–98.
4. Lynch TJ, Bell DW, Sordella R, et al. Activating mutations in the epidermal growth factor receptor underlying responsiveness of non-small-cell lung cancer to gefitinib. *N Engl J Med.* 2004; 350:2129–2139.
5. Paez JG, Janne PA, Lee JC, et al. *EGFR* mutations in lung cancer: correlation with clinical response to gefitinib therapy. *Science.* 2004; 304:1497–1500.
6. Pao W, Miller V, Zakowski M, et al. EGF receptor gene mutations are common in lung cancers from "never smokers" and are associated with sensitivity of tumors to gefitinib and erlotinib. *Proc Natl Acad Sci USA.* 2004;101:13306–13311.
7. Kosaka T, Yatabe Y, Endoh H, et al. Mutations of the epidermal growth factor receptor gene in lung cancer: biological and clinical implications. *Cancer Res.* 2004;64:8919–8923.
8. Marchetti A, Martella C, Felicioni L, et al. *EGFR* mutations in non-small-cell lung cancer: analysis of a large series of cases and development of a rapid and sensitive method for diagnostic screening with potential implications on pharmacologic treatment. *J Clin Oncol.* 2005;23:857–865.
9. Tokumo M, Toyooka S, Kiura K, et al. The relationship between epidermal growth factor receptor mutations and clinicopathologic features in non-small cell lung cancers. *Clin Cancer Res.* 2005;11: 1167–1173.
10. Shigematsu H, Lin L, Takahashi T, et al. Clinical and biological features associated with epidermal growth factor receptor gene mutations in lung cancers. *J Natl Cancer Inst.* 2005;97:339–346.
11. Huang SF, Liu HP, Li LH, et al. High frequency of epidermal growth factor receptor mutations with complex patterns in non-small cell lung cancers related to gefitinib responsiveness in Taiwan. *Clin Cancer Res.* 2004;10:8195–8203.
12. Yang SH, Mechanic LE, Yang P, et al. Mutations in the tyrosine kinase domain of the epidermal growth factor receptor in non-small cell lung cancer. *Clin Cancer Res.* 2005;11:2106–2110.
13. Han SW, Kim TY, Hwang PG, et al. Predictive and prognostic impact of epidermal growth factor receptor mutation in non-small-cell lung cancer patients treated with gefitinib. *J Clin Oncol.* 2005; 23:2493–2501.
14. Pao W, Miller VA. Epidermal growth factor receptor mutations, small-molecule kinase inhibitors, and non-small-cell lung cancer: current knowledge and future directions. *J Clin Oncol.* 2005;23: 2556–2568.
15. Sordella R, Bell DW, Haber DA, et al. Gefitinib-sensitizing *EGFR* mutations in lung cancer activate anti-apoptotic pathways. *Science.* 2004;305:1163–1167.
16. Druker BJ, Talpaz M, Resta DJ, et al. Efficacy and safety of a specific inhibitor of the *BCR-ABL* tyrosine kinase in chronic myeloid leukemia. *N Engl J Med.* 2001;344:1031–1037.
17. Cella D, Herbst RS, Lynch TJ, et al. Clinically meaningful improvement in symptoms and quality of life for patients with non-small-cell lung cancer receiving gefitinib in a randomized controlled trial. *J Clin Oncol.* 2005;23:2946–2954.
18. Fukuoka M, Yano S, Giaccone G, et al. Multi-institutional randomized phase II trial of gefitinib for previously treated patients with advanced non-small-cell lung cancer (The IDEAL 1 Trial). *J Clin Oncol.* 2003;21:2237–2246.
19. Kris MG, Natale RB, Herbst RS, et al. Efficacy of gefitinib, an inhibitor of the epidermal growth factor receptor tyrosine kinase, in symptomatic patients with non-small cell lung cancer: a randomized trial. *JAMA.* 2003;290:2149–2158.
20. Bosari S, Marchetti A, Buttitta F, et al. Detection of *p53* mutations by single-strand conformation polymorphisms (SSCP) gel electrophoresis. A comparative study of radioactive and nonradioactive silver-stained SSCP analysis. *Diagn Mol Pathol.* 1995;4:249–255.
21. Fan X, Furnari FB, Cavenee WK, et al. Non-isotopic silver-stained SSCP is more sensitive than automated direct sequencing for the detection of *PTEN* mutations in a mixture of DNA extracted from normal and tumor cells. *Int J Oncol.* 2001;18:1023–1026.
22. Sasaki H, Endo K, Konishi A, et al. *EGFR* Mutation status in Japanese lung cancer patients: genotyping analysis using LightCycler. *Clin Cancer Res.* 2005;11:2924–2929.
23. Pan Q, Pao W, Ladanyi M. Rapid polymerase chain reaction-based detection of epidermal growth factor receptor gene mutations in lung adenocarcinomas. *J Mol Diagn.* 2005;7:396–403.
24. Mitsudomi T, Kosaka T, Endoh H, et al. Mutations of the epidermal growth factor receptor gene predict prolonged survival after gefitinib treatment in patients with non-small-cell lung cancer with postoperative recurrence. *J Clin Oncol.* 2005;23:2513–2520.

Sentinel node navigation segmentectomy for clinical stage IA non–small cell lung cancer

Hiroaki Nomori, MD, PhD,[a] Koei Ikeda, MD, PhD,[a] Takeshi Mori, MD,[a] Hironori Kobayashi, MD,[a] Kazunori Iwatani, MD,[a] Koichi Kawanaka, MD, PhD,[b] Shinya Shiraishi, MD, PhD,[b] and Toshiaki Kobayashi, MD, PhD[c]

From right to left: Drs Nomori, Mori, and Ikeda. The Bronze statue is Dr Shibasaburo Kitasato

Objective: Intraoperative frozen section examination of sentinel lymph nodes was conducted to determine the final indication for segmentectomy for clinical T1 N0 M0 non–small cell lung cancer.

Methods: Between April 2005 and July 2006, 52 patients with clinical T1 N0 M0 non–small cell lung cancer were prospectively treated by segmentectomy with sentinel node identification. The day before surgery, technetium-99m tin colloid was injected into the peritumoral region. After segmentectomy and lymph node dissection, sentinel nodes identified by measuring radioactive tracer uptake were examined for intraoperative frozen sections, which were serially cut 2 to 3 mm in thickness. When sentinel node metastasis was observed, segmentectomy was converted to lobectomy.

Results: Sentinel nodes were identified in 43 (83%) patients. The average number of sentinel nodes was 1.6 ± 0.9 (range: 1–5) per patient. Of 3 patients with metastatic sentinel lymph nodes, 2 underwent lobectomy and 1 larger segmentectomy. None of the other 40 patients had metastatic sentinel lymph nodes and therefore they were treated with segmentectomy. Pathologic staging with permanent sections was N0 in all of the 40 patients. On the other hand, in 9 patients whose sentinel nodes could not be identified, intraoperative frozen sections were required for 5.4 ± 2.3 lymph nodes, which was significantly more than 1.6 ± 0.9 in the 43 patients with sentinel node identification ($P < .001$).

Conclusion: Sentinel node identification is useful to determine the final indication of segmentectomy for clinical T1 N0 M0 non–small cell lung cancer by targeting the lymph nodes needed for intraoperative frozen section diagnosis.

From the Departments of Thoracic Surgery[a] and Radiology,[b] Graduate School of Medical Sciences, Kumamoto University, Honjo, Kumamoto, Japan; and the Department of Assistive Diagnostic Technology,[c] National Cancer Center Hospital, Tokyo, Japan.

This work was supported, in part, by Grant-in-Aid from the Ministry of Health, Labor, and Welfare, Japan.

Received for publication Aug 20, 2006; revisions received Oct 7, 2006; accepted for publication Oct 23, 2006.

Address for reprints: Hiroaki Nomori, MD, PhD, Department of Thoracic Surgery, Graduate School of Medical Sciences, Kumamoto University, 1-1-1 Honjo, Kumamoto 860-8556, Japan (E-mail: hnomori@qk9.so-net.ne.jp).

J Thorac Cardiovasc Surg 2007;133:780-5

0022-5223/$32.00

doi:10.1016/j.jtcvs.2006.10.027

GTS

In 1995, the Lung Cancer Study Group[1] conducted a prospective randomized controlled trial of limited resection versus lobectomy for clinical T1 N0 M0 non–small cell lung cancer (NSCLC) and concluded that the former was inferior to the latter regarding local recurrence and survival. However, the limited resection group in the study included both segmentectomy and wedge resection, and the curability for T1 N0 M0 NSCLC differed between the two procedures. On the other hand, there have been several reports describing that survivals were similar between patients treated with segmentectomy and those with lobectomy.[2-7]

The most important issue regarding segmentectomy versus lobectomy is whether postoperative local recurrence is increased. Whereas Warren and Faber[8] reported local recurrence in 15 (22.7%) of 66 patients after segmentectomy versus 5 (4.9%) of 103 patients after lobectomy, other authors reported that local recurrence after segmentectomy with complete dissection of hilar and mediastinal lymph nodes was equal to that after lobectomy.[3-6] However, for determining the final indication for segmentectomy, intraoperative frozen sections must be examined for all of the hilar

Abbreviations and Acronyms

CT = computed tomography
FDG-PET = fluorodeoxyglucose–positron emission tomography
NSCLC = non–small cell lung cancer
SN = sentinel node
SPECT = single photon emission computed tomography

and lobe-specific mediastinal lymph nodes to confirm the intraoperative N staging to be N0.[3-6]

A sentinel node (SN) is defined as the first lymph node within the lymphatic basin reached by lymph draining from the primary lesion. Recently, SNs have been identified by a radioactive tracer with or without dye during surgery for melanoma, breast cancer, gastrointestinal cancer, and lung cancer to reduce lymph node dissection.[9-14] We[13,14] previously reported that SN identification with technetium-99m tin colloid could establish the first site of nodal metastasis in NSCLC.

In the present study, we used SN identification to target the lymph nodes submitted for intraoperative frozen section diagnosis, which might determine the indication of segmentectomy. In addition, unlike Tsubota,[3] Okada,[4] Yoshikawa,[5] and their associates, who proposed that the indication for segmentectomy was T1 N0 M0 NSCLC less than 2 cm in size, we proposed that it was T1 N0 M0 NSCLC without size limitation. Because SN identification served as the final indication of segmentectomy, we named the procedure "sentinel node navigation segmentectomy."

Patients and Methods

Eligibility

The study protocol for SN navigation segmentectomy was approved by the Ethics Committee of Kumamoto University Hospital in March 2005. Informed consent was obtained from all patients after discussing the risks and benefits of the proposed surgery with their surgeons.

Patients

Between April 2005 and July 2006, 103 patients with NSCLC underwent surgical treatment. Of these, 73 patients had stage c-T1 N0 M0 cancer according to the findings of both computed tomography (CT) and fluorodeoxyglucose–positron emission tomography (FDG-PET). SN navigation segmentectomy was prospectively performed when (1) c-T1 N0 M0 NSCLC was identified in the peripheral lung; (2) the tumor on CT was more than 2 cm away from the pulmonary vein running at the boundary of the affected segment; (3) intraoperative frozen sections of SN showed no metastasis; (4) the surgical margin was intraoperatively found to be more than 2 cm from the tumor; and (5) tumors located centrally within the inner one third of the lung or in the right middle lobe were excluded. The stage of disease was based on the TNM classification of the International Union Against Cancer.[15] The lymph node nomenclature used was according to the lymph node map of Naruke and associates,[16] which was approved by the Japan Lung Cancer Society (Table 1).

TABLE 1. Lymph node nomenclature

N2 node	N1 node
Superior mediastinal	Hilar
No. 1. Highest mediastinal	No. 10. Hilar
No. 2. Paratracheal	No. 11. Interlobar
No. 3. Pretracheal	No. 12. Lobar
No. 4. Tracheobronchial	
Aortic	Intrapulmonary
No. 5. Botallo	No. 13. Segmental
No. 6. Para-aortic	No. 14. Subsegmental
Inferior mediastinal	
No. 7. Subcarinal	
No. 8. Paraesophageal	
No. 9. Pulmonary ligament	

Administration of Radioactive Colloid

The day before surgery, a 23-gauge needle was introduced into the peritumoral region under single photon emission computed tomography/computed tomography (SPECT/CT) system guidance, which incorporates a gantry-free SPECT with dual-head detectors (Skylight; ADAC Laboratories, Milpitas, Calif) and an 8 multidetector CT scanner (Light-Speed Ultra; General Electrics, Milwaukee, Wis). Technetium tin colloid (6–8 mCi) suspended in a 1- to 1.5-mL volume was injected in a single shot. SPECT/CT was performed 5 minutes after the injection and the next morning just before the operation.

SN Identification

The radioactivity of the resected lymph nodes was counted with a handheld gamma probe (Navigator; Auto Suture Japan, Tokyo, Japan). The radioactivity was measured for a 10-second period. SN was defined as any node for which the count was more than 5 times the radioactivity of the resected tissue with the lowest count.

SN Navigation Segmentectomy

Under thoracotomy, SN navigation segmentectomy was performed as follows: (1) Pulmonary arteries and bronchi of the affected segments were cut at the hilum; (2) pulmonary veins along the boundary of segments were isolated from the center to periphery; (3) the affected segments along the pulmonary veins were resected with staplers; (4) the hilar and systematic mediastinal lymph nodes were dissected; (5) the radioactivity of dissected lymph nodes was counted for SN identification; (6) SNs were examined by intraoperative frozen sections, which were serially cut 2 to 3 mm in thickness; (7) if the intraoperative frozen sections of the SN showed no metastasis, the operation was completed with segmentectomy; (8) if the sections of the SN showed metastasis, lobectomy was performed; and (9) if the SN could not be identified because radioactivity of the lymph nodes was low, all of the hilar and lobe-specific mediastinal lymph nodes were submitted for

GTS

TABLE 2. Sites of segmentectomy

Segment	No. of patients	Segment	No. of patients
Right		Left	
Upper lobe		Upper lobe	
S1	3	S1 + 2	4
S2	2	S3	2
S1 + S2	2	S1 + 2 + 3	9
S3	2	S4 + 5	7
S3 + S2b	1		
S2 + S3a	1		
Lower lobe		Lower lobe	
S6	4	S6	3
S7 + 8	1	S8	1
S8	1	S8 + 9	2
S9 + S10	2	S9 + 10	1
S7–10	1	S10	1
S6 + S9 + S10	1	S8–10	1
Total	21		31

Right upper lobe: *S1*, apical; *S2*, anterior; *S3*, posterior. Right lower lobe: *S6*, apical; *S7*, medial; *S8*, anterior; *S9*, lateral; *S10*, posterior. Left upper lobe: *S1+2*, apical posterior; *S3*, apical anterior; *S4*, superior lingular; *S5*, inferior lingular. Left lower lobe: *S6*, apical; *S8*, anterior; *S9*, lateral; *S10*, posterior.

TABLE 3. Characteristics of patients with and without sentinel node identification

	Sentinel lymph node	
	Identifiable	Nonidentifiable
Mean age (y)	69 ± 7	71 ± 7
Sex		
Male	26	8
Female	17	1
Mean tumor size (cm)	1.9 ± 0.7	2.1 ± 0.7
Histologic type		
Adenocarcinoma	37	6
Squamous cell carcinoma	4	2
Adenosquamous carcinoma	2	1
No. of lymph nodes submitted for intraoperative frozen diagnosis	1.6 ± 0.9	5.4 ± 2.3*
Pathologic TNM		
T1 N0 M0	39	9
T2 N0 M0	1	0
T1 N1 M0	1	0
T2 N1 M0	1	0
T1 N2 M0	1	0
Total	43	9

*$P < .001$.

intraoperative frozen section. Lobe-specific lymph nodes were defined as follows: No. 3 and No. 4 for the right upper lobe, No. 5 for the left upper lobe, and No. 7 for the lower lobe of both sides.[17]

Primary End Points of the Study

Primary end points of the study are as follows: (1) Can SN identification diagnose pathologic N stage during segmentectomy? (2) Are the survival and local recurrence after SN navigation segmentectomy similar to those after lobectomy?

Statistical Analysis

All data were analyzed for significance by the 2-tailed Student *t* tests. All values in the text and tables are given as mean ± SD.

Results

Operative procedures for the 73 patients with c-T1 N0 M0 were lobectomy in 12 patients, segmentectomy in 52, and wedge resection in 9. The reasons for conducting lobectomy in the 12 patients were as follows: (1) tumors in the right middle lobe in 5 patients; (2) tumors located centrally in 5 patients; (3) multiple lesions in the same lobe in 1 patient; and (4) thoracoscopic lobectomy as requested by the patient. As a result, 52 patients were consecutively enrolled for SN navigation segmentectomy. Table 2 shows the sites of segmentectomy for the 52 patients. The average number of dissected lymph node stations and lymph nodes per patient was 6 ± 1.8 stations and 12.5 ± 5.9 lymph nodes, respectively. Among the 52 patients, SNs could be identified in 43 (83%). The time needed for SN identification was within 5 minutes in each patient. The characteristics of the 43 patients with SN identification and of the 9 patients without are shown in Table 3. Average tumor size on CT was 1.9 ± 0.7 cm (range: 0.8–3.0 cm) and 2.1 ± 0.7 cm (range: 1.4–3.0 cm) in the patients with and without SN identification, respectively. Seventeen (40%) of the 43 patients with SN identification and 4 (44%) of 9 patients without had tumors larger than 2 cm. Pathologic tumor stages in the 43 patients with SN identification were T1 N0 M0 in 39, T2 N0 M0 in 1, T1 N1 M0 in 1, T2 N1 M0 in 1, and T1 N2 M0 in 1, whereas the stage in all 9 patients without SN identification was p-T1 N0 M0. The tumors in 2 patients were pathologically classified as T2; one tumor was spread over the pleura and the other was more than 3 cm in size in the permanent section. The average number of lymph nodes submitted for intraoperative frozen section examination was significantly less in the 43 patients with SN identification (1.6 ± 0.9 [range: 1–5] per patient) than in the 9 patients without SN identification (5.4 ± 2.3 [range: 3–10] per patient) ($P < .001$).

Table 4 shows the SN identified in the hilar lymph node stations. The number of stations having SN increased in numeric order from No. 10 to 13 stations. In the mediastinal lymph node stations, the SN was identified in 15 of the 43 patients (35%). Eleven of the 15 patients had SNs in both the hilar and mediastinal lymph node stations, whereas the remaining 4 patients had SNs only in the mediastinum. The distribution of mediastinal SNs is shown in Table 5, which

GTS

TABLE 4. Sentinel lymph node mapping in the hilar lymph node stations

Station	Sentinel nodes	
	No. of patients	Percent
10	7/3	16.3
11	7/43	16.3
12	12/43	27.9
13	22/43	51.2

TABLE 5. Sentinel nodes at the mediastinum in each lobe

Tumor location	Station of mediastinal SN	No. of patients	Percent
RUL	3 or 4	3/10	30.0
RLL	3 or 4	2/9	22.2
	7 and 3	1/9	11.2
LUL	5	8/18	44.4
LLL	7	2/6	33.3

SN, Sentinel node; *RUL*, right upper lobe; *RLL*, right lower lobe; *LUL*, left upper lobe; *LLL*, left lower lobe.

was lobe-specific; that is, 3 of the 10 patients with primary tumor in the right upper lobe had SN in No. 3 or 4 stations; 3 of the 9 patients with primary tumor in the right lower lobe had SN in No. 7, 3, or 4 stations; 8 of the 18 patients with primary tumor in the left upper lobe had SN in No. 5 station; and 2 of the 6 patients with primary tumor in the left lower lobe had SN in No. 7 station.

In 3 (7%) of the 43 patients with SN identification, metastasis was found in the SN by intraoperative frozen section (Table 6). For 2 of the 3 patients (patients 1 and 2), operative procedures were converted to lobectomy. The operative procedure for the remaining patient (patient 3) was converted from posterior apical segmentectomy to larger segmentectomy (upper division segmentectomy, but not to upper lobectomy), because of his age (80 years old). Pathologic N stages were N1 in 2 patients and N2 in 1 patient. Although both patients 1 and 2 had metastasis only in the SN, patient 3 had metastasis in both SN (No. 5) and non-SN (Nos. 12 and 13). Tumors in all of the other 40 patients were classified as p-N0 by permanent sections.

There were no complications associated with radioisotope injection necessitating tube drainage, such as bleeding or severe pneumothorax. One patient had empyema 3 days after segmentectomy, which was cured by drainage and antibiotics on the 23rd postoperative day. There were no the other major complications associated with segmentectomy, including prolonged air leakage of more than 5 days. The postoperative follow-up was performed by chest and abdominal CT and brain magnetic resonance imaging every 3 months after the operation. No patients were lost to follow-up. The mean follow-up period after surgery in the 52 patients was 8 months (range: 1–15 months). Postoperative recurrence occurred in 1 patient, who underwent an apical segmentectomy of the right lower lobe for adenosquamous carcinoma 2.9 cm in size. The recurrence was at 5 months after segmentectomy, at the extraregional lymph node for tumor in the right lower lobe, that is, at the interlobar lymph node (No. 11) between the right upper lobe and middle lobe, and treated by completion pneumonectomy. During the segmentectomy of this patient, No. 13 and No. 4 were identified as SNs, which showed no metastasis in intraoperative frozen sections. The patient is now alive 11 months after the completion pneumonectomy without recurrence. The other 51 patients are also now alive without recurrence.

Discussion

The present study shows that the SN navigation segmentectomy using radioisotope tracers could increase the accuracy of intraoperative N staging and could serve as the final indication for segmentectomy. In the 3 patients with N1 or N2 disease, intraoperative frozen sections of SNs showed metastasis, which suggested the need for lobectomy. In 9 segmentectomy-treated patients whose SNs could not be identified, all hilar and lobe-specific lymph nodes were required for diagnosis, a significantly larger number than in the 43 patients whose SNs could be identified. SN identification therefore could determine a final indication for segmentectomy by targeting the lymph nodes needed for intraoperative frozen section diagnosis. In addition, serial sections of SNs during surgery might find micrometastasis more easily than single section in each of a larger number of lymph nodes.

Although the postoperative follow-up period is still short, 1 patient had local recurrence 5 months after segmentectomy. The recurrence site of this patient, however, was the extraregional lymph node. In addition, the histologic type of this patient was adenosquamous carcinoma, which is known to have poorer prognosis than other types of NSCLC.[18,19] We therefore consider that the patients with clinical T1 N0 M0 NSCLC of high malignant grade, such as adenosquamous carcinoma, large cell neuroendocrine carcinoma, adenocarcinoma with high FDG uptake on PET, and NSCLC with high carcinoembryonic antigen serum level, would be preferably treated by lobectomy rather than segmentectomy, even if the intraoperative lymph node staging is N0.

Skip metastasis to the mediastinal lymph nodes has been reported to occur in 20% to 40% of patients with NSCLC,[17,20] which could be because some lymphatic flow from the lung goes directly to the mediastinum through the pleura and not to the hilar lymph node stations.[21] The present study showed that SNs were identified in the mediastinum in 15 (35%) of 43 patients and the lymphatic route to each mediastinal lymph node station was lobe-specific.

TABLE 6. Patients who were converted to major lung resection

Patient No.	Age/sex	Histologic type	Planned segmentectomy	SN with metastasis	Converted procedure	Pathologic TNM
1	70/M	Ad	Apical segment of RLL	No. 13	Lobectomy	T1 N1 M0
2	72/M	Ad	Apical segment of RLL	No. 11	Lobectomy	T2 N1 M0
3	80/M	Ad	Posterior apical segment of LUL	No. 5	Upper division segmentectomy	T1 N2 M0

SN, Sentinel node; *Ad*, adenocarcinoma; *RLL*, right lower lobe; *LUL*, left upper lobe.

Therefore, to determine the intraoperative indication for segmentectomy without using SN identification, not only hilar lymph nodes but also lobe-specific mediastinal lymph nodes should be submitted for intraoperative frozen section diagnosis. The SN identification can target the lymph nodes among those.

The identification rate of SNs was 83% in the present study, as it was in the data of previous reports by several authors, that is, 63% to 82%.[12-14] We[14] previously reported the results of SN identification in 104 patients with clinical stage I NSCLC. Of the 104 patients, 15 patients had N1 or N2 disease. Although SN could be found to have metastases during the operation in 13 (87%) of those 15 patients, it produced false negative results in the remaining 2 patients. One of the 2 patients had T2 tumor and metastasis in the No. 12 nodal station, and the other had T1 tumor and metastasis in the No. 14 nodal station, which could not be identified as SN by our procedure because of its intrapulmonary location. We therefore believe that SN could be identified by our procedure in most of the patients with T1 N0 M0 NSCLC.

Although it has been reported that 20% to 25% of patients with clinical stage I disease have mediastinal lymph node metastasis,[22,23] the present study showed only 3 (6%) of 52 patients with N1 or N2 disease. Our procedure for lymph node dissection was systematic and then yielded 6 ± 1.8 nodal stations and 12.5 ± 6 lymph nodes to be dissected per patient. The low number of patients with N1 or N2 disease in the present study is probably due to the institutional setting; that is, most lung cancers in our patients were found by routine CT examination, resulting in a higher rate of early-stage NSCLC than usual.

The Lung Cancer Study Group study in 1995 (the only prospective randomized trial of lobectomy versus limited resection for T1 N0 NSCLC) reported that limited resection was inferior to lobectomy regarding death rate and local recurrence.[1] However, the study included a significant number (33%) of wedge resections in the limited resection group and did not analyze the results of segmentectomy. In addition, compared with clinical staging in 1995 when the Lung Cancer Study Group study was reported, it is now more accurate because of improved CT and FDG-PET technology. Therefore, a prospective randomized trial of lobectomy versus segmentectomy should be performed for c-T1 N0 M0 NSCLC. The SN navigation segmentectomy, which can target lymph nodes for intraoperative frozen section diagnosis, is a reasonable procedure for determining the final indication of segmentectomy.

GTS

References

1. Lung Cancer Study Group, Ginsberg RH, Rubinstein LV. Randomized trial of lobectomy versus limited resection for T1N0 non–small cell lung cancer. *Ann Thorac Surg.* 1995;60:615-23.
2. Jensik RJ, Faber LP, Milloy FJ, Monson DO. Segmental resection for lung carcinoma. *J Thorac Cardiovasc Surg.* 1973;66:563-72.
3. Tsubota N, Ayabe K, Doi O, Mori T, Namikawa S, Taki T, et al. Ongoing prospective study of segmentectomy for small lung tumors. *Ann Thorac Surg.* 1998;66:1787-90.
4. Okada M, Yoshikawa K, Hatta T, Tsubota N. Is segmentectomy with lymph node assessment an alternative to lobectomy for non–small cell lung cancer of 2 cm or smaller? *Ann Thorac Surg.* 2001;71:956-61.
5. Yoshikawa K, Tsubota N, Kodama K, Ayabe H, Taki T, Mori T. Prospective study of extended segmentectomy for small lung tumors: the final report. *Ann Thorac Surg.* 2002;73:1055-9.
6. Kodama K, Doi O, Higashiyama M, Yokouchi H. Intentional limited resection for selected patients with T1 N0 M0 non–small cell lung cancer. *J Thorac Cardiovasc Surg.* 1997;114:347-53.
7. Harada H, Okada M, Sakamoto T, Matsuoka H, Tsubota N. Functional advantage after radical segmentectomy versus lobectomy for lung cancer. *Ann Thorac Surg.* 2005;80:2041-5.
8. Warren WH, Faber LP. Segmentectomy versus lobectomy in patients with stage I pulmonary carcinoma: five-year survival and patterns of intrathoracic recurrence. *J Thorac Cardiovasc Surg.* 1994;107:1087-93.
9. Tafra L, Lannin DR, Swanson MS, Eyk JJV, Verbanac KM, Chua AN, et al. Multicenter trial of sentinel node biopsy for breast cancer using both technetium sulfur colloid and isosulfan blue dye. *Ann Surg.* 2001;233:51-9.
10. Morton DL, Thompson JF, Essner R, Elashoff R, Stern SL, Nieweg OE, et al. Validation of the accuracy of intraoperative lymphatic mapping and sentinel lymphadenectomy for early-stage melanoma. *Ann Surg.* 1999;230:453-65.
11. Kitagawa Y, Fujii H, Mukai M, Kubota T, Ando N, Watanage M, et al. The role of the sentinel lymph node in gastrointestinal cancer. *Surg Clin North Am.* 2000;80:1799-809.
12. Liptay MJ, Masters GA, Winchester DJ, Edelman BL, Carrido BJ, Hirshctritt TR, et al. Intraoperative radioisotope sentinel lymph node mapping in non–small cell lung cancer. *Ann Thorac Surg.* 2000;70:384-90.
13. Nomori H, Horio H, Naruke T, Orikasa H, Yamazaki K, Suemasu K. Use of technetium-99m tin colloid for sentinel lymph node identification in non–small cell lung cancer. *J Thorac Cardiovasc Surg.* 2002;124:486-92.
14. Nomori H, Watanabe K, Ohtsuka T, Naruke T, Suemasu K. In vivo identification of sentinel lymph nodes for clinical stage I non–small cell lung cancer for abbreviation of mediastinal lymph node dissection. *Lung Cancer.* 2004;46:49-55.
15. Sobin LH, Wittekind CH, editors. UICC: TNM classification of malignant tumors. 6th ed. New York: John Wiley & Sons; 2002.

16. Naruke T, Suemasu K, Ishikawa S. Lymph node mapping and curability at various levels of metastasis in resected lung cancer. *J Thorac Cardiovasc Surg.* 1978;76:832-9.
17. Naruke T, Tsuchiya R, Kondo H, Nakayama H, Asamura H. Lymph node sampling in lung cancer: how should it be done? *Eur J Cardiothorac Surg.* 1999;16:S17-24.
18. Shimizu J, Oda M, Hayashi Y, Nonomura A, Watanabe Y. A clinicopathologic study of resected cases of adenosquamous carcinoma of the lung. *Chest.* 1996;109:9889-94.
19. Nakagawa K, Yasumitsu T, Fukuhara K, Shiono H, Kikui M. Poor prognosis after lung resection for patients with adenosquamous carcinoma of the lung. *Ann Thorac Surg.* 2003;75:1740-4.
20. Okada M, Tsubota N, Yoshimura M, Miyamoto Y, Matsuoka H. Prognosis of completely resected pN2 non–small cell lung carcinomas: what is the significant node that affects survival? *J Thorac Cardiovasc Surg.* 1999;118:270-5.
21. Riquet M, Hidden G, Debesse B. Direct lymphatic drainage of lung segments to the mediastinal nodes. *J Thorac Cardiovasc Surg.* 1989;97:623-32.
22. Seely JM, Mayo JR, Miller RR, Muller NL. T1 lung cancer: prevalence of mediastinal node metastases and diagnostic accuracy of CT. *Radiology.* 1993;186:129-32.
23. Heavey LR, Glazer GM, Gross BH, Francis IR, Orringer MB. The role of CT in staging radiographic T1N0M0 bronchogenic cancer. *AJR.* 1986;146:285-90.

Journal of Pathology
J Pathol 2007; **212**: 38–46
Published online 16 March 2007 in Wiley InterScience
(www.interscience.wiley.com) **DOI:** 10.1002/path.2150

Original Paper

Class A scavenger receptor (CD204) attenuates hyperoxia-induced lung injury by reducing oxidative stress

H Kobayashi,[1–3] N Sakashita,[1] T Okuma,[1] Y Terasaki,[1] K Tsujita,[1] H Suzuki,[4] T Kodama,[5] H Nomori,[2] M Kawasuji[3] and M Takeya[1]*

[1] *Department of Cell Pathology, Graduate School of Medical Sciences, Kumamoto University, Kumamoto, Japan*
[2] *Department of Thoracic Surgery, Graduate School of Medical Sciences, Kumamoto University, Kumamoto, Japan*
[3] *Department of Cardiovascular Surgery, Graduate School of Medical Sciences, Kumamoto University, Kumamoto, Japan*
[4] *National Research Center for Protozoan Diseases, Obihiro University of Agriculture and Veterinary Medicine, Hokkaido, Japan*
[5] *Department of Molecular Biology and Medicine, Research Center for Advanced Science and Technology, The University of Tokyo, Tokyo, Japan*

*Correspondence to:
M Takeya, MD, PhD,
Department of Cell Pathology,
Graduate School of Medical
Sciences, Kumamoto University,
1-1-1 Honjo, Kumamoto
860-8556, Japan.
E-mail:
takeya@kaiju.medic.kumamoto-u.ac.jp

No conflicts of interest were declared.

Received: 6 November 2006
Revised: 30 December 2006
Accepted: 26 January 2007

Abstract

To clarify the role of macrophage class A scavenger receptors (SR-A, CD204) in oxidative lung injury, we examined lung tissue of SR-A deficient ($SR\text{-}A^{-/-}$) and wild-type ($SR\text{-}A^{+/+}$) mice in response to hyperoxic treatment. Protein levels of bronchoalveolar lavage fluid (BALF) and pulmonary oedema (wet : dry weight ratios) were higher in $SR\text{-}A^{-/-}$ mice than those in $SR\text{-}A^{+/+}$ mice. Cumulative survival was significantly decreased in $SR\text{-}A^{-/-}$ mice. However, there were no differences in BALF macrophage and neutrophil count between the two groups. Real-time reverse transcriptase-polymerase chain reaction (RT-PCR) revealed that messenger RNA (mRNA) levels of the inducible nitric oxide synthase (iNOS) were increased during hyperoxic injury, and this increase was more prominent in $SR\text{-}A^{-/-}$ mice. Expression levels of iNOS in alveolar macrophages after hyperoxia *in vivo* and *in vitro* were higher in $SR\text{-}A^{-/-}$ macrophages compared with $SR\text{-}A^{+/+}$ macrophages. Immunohistochemistry using anti-nitrotyrosine antibodies revealed distinctive oxidative stress in the injured lung in both groups, but it was more remarkable in the $SR\text{-}A^{-/-}$ mice. After hyperoxic treatment, pulmonary mRNA levels of tumour necrosis factor-α(TNF-α) were elevated more rapidly in $SR\text{-}A^{-/-}$ mice than in $SR\text{-}A^{+/+}$ mice. Together these results suggest that SR-A expression attenuates hyperoxia-induced lung injury by reducing macrophage activation.

Keywords: class A scavenger receptor (CD204); macrophages; hyperoxic lung injury; inducible nitric oxide synthase; tumour necrosis factor-α; oxidative stress

Introduction

Oxidative stress is a major pathogenic factor for a wide variety of diseases, which broadly regulates tissue and cell injury as well as inflammatory responses [1]. A clinical manifestation of oxidative stress is hyperoxic lung injury [2–4], caused by prolonged high-dose oxygen supplementation producing acute pulmonary injury with lung oedema and alveolar damage. Hyperoxia induces the production of pro-inflammatory cytokines such as tumour necrosis factor-alpha (TNF-α), interleukin-6 (IL-6), and interferon γ from alveolar macrophages [5–7]. These cytokines, especially TNF-α, activate the production of inducible nitric oxide synthase (iNOS) in injured tissue to cause a nitric oxide burst [8]. Overexpression of iNOS during the course of hyperoxic lung injury is a major cause of explosive nitric oxide production, which produces strong oxidative stress [9,10]. Activated alveolar macrophages and type II pneumocytes in hyperoxic lung tissue release both nitric oxide and superoxide, which react with each other to form peroxynitrite anion. Peroxynitrite is a chemically active oxidizing molecule that causes serious oxidative damage to pulmonary epithelia and endothelia, producing acute alveolar damage and pulmonary oedema [11]. Nitric oxide and superoxide clearly play key roles as mediators in the pathway from oxidative stress to hyperoxic pulmonary damage *in situ*.

Scavenger receptors are essential for macrophage function. Class A scavenger receptors (SR-As) are one of the principal receptors of macrophages. These receptors bind various negatively-charged macromolecules, such as modified low-density lipoprotein, advanced glycation end-products, denatured collagen, and asbestos bodies [12–16]. SR-As are multifunctional molecules; in addition to their major function of eliminating their target ligands, they are also

involved in cell adhesion, host defence, the removal of apoptotic cells, neural disorders, and cytokine production [12–14,17]. Recently, it has been reported that SR-A molecules regulate the production of pro-inflammatory cytokines such as TNF-α, raising the possibility that SR-A is a potential regulatory factor of oxidative stress and concomitant inflammation [18–20].

The aim of this study was to examine the role of SR-A on inflammatory responses and oxidative stress. We chose hyperoxia-induced acute lung injury as an organ-specific oxidative stress model. We found that SR-A deficiency exacerbates oxidative lung injury. After a series of experiments, we confirmed that intrapulmonary SR-A expression reduces macrophage activation by suppressing the production of pro-inflammatory cytokines and nitric oxide from macrophages *in situ*.

Materials and methods

Animals

SR-A-deficient male mice, 8–12 weeks of age, with a C57BL/6J genetic background as described previously [12,13], were used in all experiments. Wild-type mice with identical genetic backgrounds were employed as controls (Clea Japan, Tokyo, Japan). All mice were maintained under specific-pathogen-free conditions in the Animal Resource Facility of Kumamoto University, which approved all of the *in vivo* experiments performed in this study.

Hyperoxic lung injury

Mice were placed in an airtight stainless steel chamber ($35 \times 45 \times 55$ cm^3; Natsume Seisakusyo Co, Ltd, Tokyo, Japan), with ducts connecting to an airflow controller and a plastic window for observation. Based on our previous report [21] and our preliminary experiments, 85% oxygen-containing air was employed as a hyperoxic challenge to animals. The oxygen concentration in the chamber was maintained at 85.0–88.0% at a temperature of 22–24 °C. Mice had free access to food and water in the chamber. Mice without hyperoxic treatment were designated as 'day 0'.

Bronchoalveolar lavage (BAL)

Before or after hyperoxic challenge, mice were anaesthetized with pentobarbital sodium (Dainabot, Osaka, Japan) and a 20-gauge catheter (Becton Dickinson, Franklin Lakes, NJ, USA) was inserted into the trachea through a small incision. Airspaces were lavaged twice with sterile saline (0.75 ml each; total volume 1.5 ml) and the recovery volume of BAL fluid (BALF) was 1.3–1.4 ml. BALF was centrifuged at 1500 rpm for 5 min at 4 °C. The total protein concentration in the supernatant was determined by a Micro BCA Protein Assay Kit (Pierce, Rockford, IL, USA). Cytospin preparation was used to determine differential cell counts. For neutrophil counting, the slides were stained using a Diff-Quick stain kit (Kokusai Shiyaku, Kobe, Japan) as previously described [22]. The slides were stained with anti-pan-macrophage antibody FA11 (anti-CD68; Serotec, Oxford, UK). The number of inflammatory cells per mm^2 was counted in ten areas randomly selected under high-power magnification (×400). After calculating mean cell counts, the number of macrophages and neutrophils in BALF per mouse was determined [21].

Wet to dry lung weight ratio

To evaluate pulmonary damage, we employed wet to dry lung weight ratio as a marker of pulmonary oedema associated with hyperoxic lung injury. At days 0 and 4 of hyperoxic treatment, the left lungs were collected and weighed. Afterwards, the lungs were desiccated in an oven for 5 h at 130 °C, weighed again, and the wet to dry weight ratio was calculated.

Cryosection preparation

For biochemical analysis, left lungs were removed, frozen in liquid nitrogen, and stored at −80 °C until use. After removing the left lung, ligation of the left main bronchus, *en bloc* resection of the heart, right lung, and chest wall was performed to avoid mechanical damage to the right lung surface. Right lungs were inflated with 4% paraformaldehyde at a pressure of 25 cmH_2O and further fixed by immersing in 4% paraformaldehyde for 6 h at 4 °C. After fixation, samples were rinsed with a graded series of sucrose in phosphate-buffered saline (PBS) every 6 h and then embedded into OCT compound (Sakura Finetek, Tokyo, Japan) and frozen in liquid nitrogen. Cryosections (6 μm thick) were cut, mounted on silane-coated slide, and dried in an air flow. One cryosection per sample was stained with hematoxylin and eosin, and the remaining sections were used for immunohistochemical staining.

Hyperoxic cell culture

Cells collected from BALF were suspended in RPMI 1640 medium supplemented with 10% fetal bovine serum (JRH Biosciences, Lenexa, KS, USA) and penicillin/streptomycin (Invitrogen, Carlsbad, CA, USA), and incubated for 2 h in a 5% CO_2 incubator to allow cell adherence. Non-adherent cells were removed by gentle washes with PBS. The remaining cells, which were mainly alveolar macrophages, were exposed to hyperoxic air containing 5% CO_2, 85% O_2, and 10% room air or normoxic air containing 5% CO_2 and 95% room air using a hyperoxic tissue culture incubator (APM-30D, ASTEC, Fukuoka, Japan).

Antibodies

To detect macrophages in injured lungs, anti-mouse CD68 antibodies (FA11; Serotec, Oxford, UK) were

used. SR-As were detected by biotinylated mouse anti-human SR-A monoclonal antibodies (SRA-E5; Transgenic Inc, Kumamoto, Japan) that cross-reacted with mouse SR-A [23]. Rabbit polyclonal anti-iNOS (Lab Vision, Fremont, CA, USA) and anti-nitrotyrosine (Sigma, St Louis, MO, USA) antibodies were employed to evaluate oxidative stress using histological techniques.

Immunohistochemistry

Cryosections were rinsed with PBS at 4 °C and then immersed in methanol containing 0.3% H_2O_2 for 30 min to inactivate endogenous peroxidase activity. Sections were then incubated in 5% normal goat serum for 30 min before overnight incubation with primary antibodies at 4 °C. After removal of excess primary antibodies by three washes with PBS, the samples were incubated with an appropriate horseradish peroxidase-linked anti-immunoglobulin [$F(ab')_2$] (Nichirei, Tokyo, Japan) or horseradish peroxidase-linked streptoavidin (Nichirei) solution for 60 min at room temperature. Specific immunoreactivity was visualized by 3,3′-diaminobenzidine–H_2O_2 solution. Cryosections were counterstained with haematoxylin or methyl green and mounted with Marinol (Mutoh Chemical Co., Tokyo, Japan). Negative controls were stained using the same procedure with the omission of primary antibodies. For immunohistochemistry, alveolar macrophages were mounted onto silane-coated glass slides and fixed with cold (4 °C) acetone for 5 min. Immunohistochemistry was performed as described above. Semi-quantitative assessment to evaluate the intensity of iNOS-specific immunohistochemical labelling (and thus iNOS expression) in alveolar macrophages was performed as follows: 0: negative; 1: weak; 2: moderate; and 3: strong. Average intensities were calculated after evaluating 100 macrophages from each mouse.

Reverse transcription-polymerase chain reaction (RT-PCR)

To detect the expression of TNF-α mRNA in lung tissue, RT-PCR was employed. Total RNA in the sample was extracted by using a RNA STAT-60™ extraction kit according to the manufacturer's protocol (Tel-Test, Inc, Friendswood, TX, USA). Five hundred nanograms of RNA was used to produce cDNA with an Ominiscript RT kit (Qiagen, Valencia, CA, USA). PCR primers for mouse TNF-α and glyceraldehyde-3-phosphate dehydrogenase (GAPDH) were purchased from Invitrogen. The sequence of primers used was as follows: TNF-α: sense 5′-GGCAGGTCTACTTTGGAGTCATTGC-3′; antisense 5′-ACATTCGAGGCTCCAGTGAATTCGG-3′; GAPDH: sense 5′-GGAAAGCTGTGGCGTGATG-3′; antisense 5′-CTGTTGCTGTAGCCGTATTC-3′. Expected PCR product sizes were 300 bp for TNF-α and 392 bp for GAPDH. The PCR reaction was carried out as follows: 15 min at 95 °C; 30 s at 94 °C; and 30 s at 60–72 °C for 40 cycles with an iCycler (Bio-Rad Laboratories, Hercules, CA, USA). PCR products were run on a 2.0% agarose gel electrophoresis and were visualized by ethidium bromide and scanned by a Gel Doc 2000 analyzer (Bio-Rad Laboratories). The level of TNF-α gene expression was semi-quantified by densitometry using a Scion Image processing and analysis program (Scion Corporation, Frederick, MD, USA). Relative expression levels were estimated by the density ratio of TNF-α to GAPDH.

Real-time RT-PCR

To estimate the expression levels of SR-A and iNOS in lung tissue, real-time RT-PCR was employed. We used an ABI PRISM 7300 sequence detection system, TAKARA Premix Ex Taq ™ (TAKARA, Shiga, Japan), and Assays-on-Demand gene expression probes (Applied Biosystems, Foster City, CA, USA). Rodent 18 S ribosomal RNA control reagent VIC (Applied Biosystems) was used as an endogenous control. To provide a relative standard curve, a serial dilution of mouse lung cDNA was prepared. The amplification cycle consisted of 10 s at 95 °C, 5 s at 95 °C, and 31 s at 60 °C. The total cycles for PCR reaction were 40. Relative quantification values of the target genes were standardized according to the value of endogenous 18 S ribosomal RNA.

Western blot analysis

Lung tissue stored at −80 °C was homogenized in solubilization buffer containing 10 mM Tris–HCl (pH 7.4), 150 mM NaCl, 1 mM EDTA, and 1% (w/v) Triton X-100. A proteinase inhibitor cocktail (Nacalai Tesque, Kyoto, Japan) was added to this buffer immediately before homogenization. Homogenates were centrifuged at 15 000 rpm at 4 °C for 30 min. The protein concentrations of the sample were determined using a Micro BCA Protein Assay Kit (Pierce). Twenty nanograms of protein was run on 10% SDS-PAGE gels and then transferred onto polyvinylidene fluoride membranes (Millipore, Billerica, MA, USA). Western blots were performed using anti-human SR-A antibodies and VECTASTAIN Elite ABC Reagents (Vector Laboratories, Burlingame, CA, USA). Immunoreaction was visualized by 3,3′-diaminobentizine–H_2O_2 solution.

Statistical analysis

All results are expressed as means ± SEM. Mann-Whitney's U-test was used for two-group comparisons. Cumulative survival rate was examined between two groups using Kaplan–Meier survival analysis and the log rank test. A value of $p < 0.05$ was considered statistically significant.

Results

Cumulative survival

To examine the role of SR-A in hyperoxia-induced lung injury, we compared the cumulative survival between SR-A$^{-/-}$ and SR-A$^{+/+}$ mice. All of the SR-A$^{-/-}$ mice died within 5 days after exposure to 85% O_2, whereas the SR-A$^{+/+}$ mice survived 1 or 2 days longer (Figure 1). No mice could survive more than 6 days. There was a significant difference in cumulative survival between the two groups. Autopsy revealed extensive pulmonary oedema with haemorrhage in both groups (data not shown), suggesting that the direct cause of death was hyperoxic acute lung injury, as indicated previously [24,25].

Cell counts in BALF

After 85% O_2 exposure, the macrophage counts in BALF were not significantly increased compared with those of 'day 0' in SR-A$^{+/+}$ and SR-A$^{-/-}$ mice, and there were no statistical differences between the two groups (Supplementary Figure 1A, available at http://www.interscience.wiley.com/jpages/0022-3417/suppmat/path.2150.html). The neutrophil counts in BALF increased gradually during hyperoxic exposure in SR-A$^{+/+}$ and SR-A$^{-/-}$ mice; however, there were no statistical differences between the two groups at individual time points (Supplementary Figure 1B, available at http://www.interscience.wiley.com/jpages/0022-3417/suppmat/path.2150.html).

Protein concentrations in BALF

After hyperoxic treatment, protein concentrations in the BALF from SR-A$^{+/+}$ mice increased gradually from day 3. By contrast, a rapid increase was observed in SR-A$^{-/-}$ mice and significant differences in the protein levels between the two groups were observed at days 3 and 4 (Figure 2). Although the protein concentration in BALF was further increased in both groups at day 5, there was no significant difference between the two groups at this time point. Most mice with hyperoxic challenge died by day 5, indicating

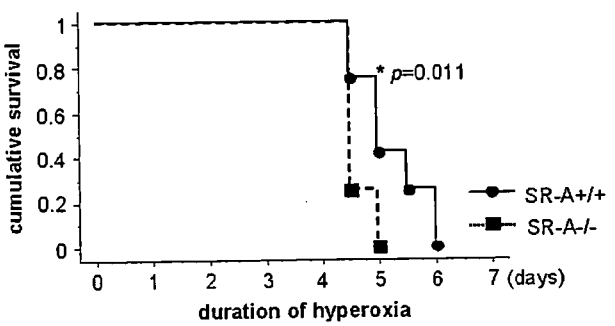

Figure 1. Cumulative survival during 85% O_2 exposure. Hyperoxic exposure causes earlier death and higher mortality in SR-A$^{-/-}$ mice than in SR-A$^{+/+}$ mice. Twelve mice in each group were studied

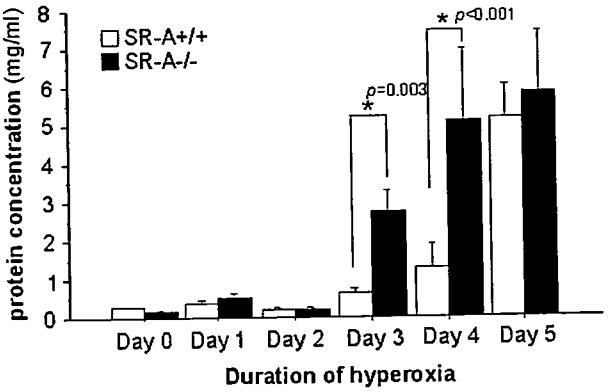

Figure 2. Total protein concentration in BAL fluid from SR-A$^{+/+}$ (open bars) and SR-A$^{-/-}$ (solid bars) mice during 85% O_2 exposure. Values are expressed as means ± SEM. Four mice per group at each time point were studied

that increased protein level in BALF may reflect lethal alveolar damage induced by hyperoxic exposure.

Wet to dry lung weight ratio

For direct evaluation of pulmonary oedema induced by hyperoxia, we examined the wet to dry weight ratio of injured lung. The wet to dry ratio for both groups was significantly increased compared with those before hyperoxic exposure. It is noteworthy that the ratio was significantly higher in SR-A$^{-/-}$ mice than in SR-A$^{+/+}$ mice at day 4 (Supplementary Figure 2, available at http://www.interscience.wiley.com/jpages/0022-3417/suppmat/path.2150.html). Histological examination confirmed severe pulmonary damage in the lungs from SR-A$^{-/-}$ mice (data not shown).

SR-A expression in hyperoxic lung injury

Exposure of SR-A$^{+/+}$ mice to 85% oxygen for 4 days resulted in augmented SR-A immunoreactivity on alveolar macrophages compared with mice without hyperoxic exposure. However, the number of FA11-positive alveolar macrophages and their staining intensity did not change between day 0 and day 4 (Figure 3A). Real-time RT-PCR and western blot revealed that the expression level of SR-A in wild-type mice increased gradually during hyperoxic exposure (Figures 3B and 3C).

Expression of iNOS and nitrotyrosine formation

Expression levels of iNOS mRNA from murine lungs at days 0 and 3 of hyperoxia were determined using real-time RT-PCR. We found significantly higher iNOS mRNA expression in SR-A$^{-/-}$ mice than in SR-A$^{+/+}$ mice (Figure 4A). Positive immunostaining for iNOS was observed in the alveolar macrophages obtained from both groups of mice exposed to high O_2 for 4 days; however, the intensity of the staining was stronger in SR-A$^{-/-}$ mice than in SR-A$^{+/+}$ mice (Figure 4B). *In vitro* exposure of alveolar

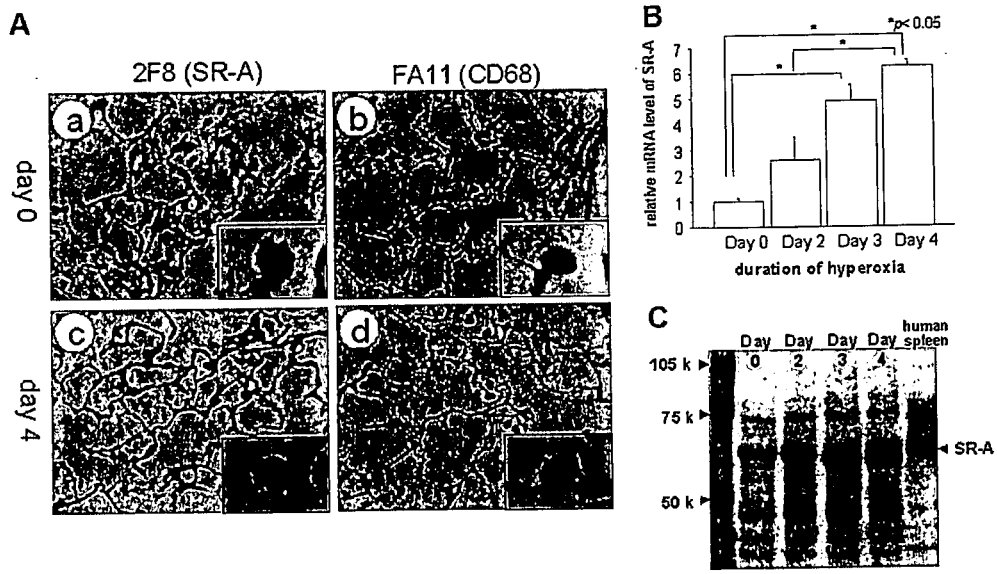

Figure 3. (A) Immunohistochemistry of SR-A (a, c) and CD68 (a general macrophage marker) (b, d) in lung tissue from SR-A$^{+/+}$ mice. Results from day 0 (a, b) and day 4 (c, d) of hyperoxia treatment are shown. Original magnification ×200. (B) SR-A mRNA levels determined by real-time RT-PCR. Total RNA was extracted from the left lungs of mice and subjected to real-time RT-PCR. Values of mRNA levels are expressed as the expression level of SR-A relative to that of 18S ribosomal RNA. Relative levels of SR-A mRNA increased in a time-dependent manner after hyperoxia treatment. Statistically significant differences between days 0 and 3, and days 0 and 4 were detected. For each time point, tissue was obtained from four mice in each group. (C) Western blot analysis of SR-A expression before and after hyperoxia treatment. After hyperoxic treatment, the left lungs of mice were homogenized in solubilization buffer and the soluble fraction was subjected to western blot analysis. In agreement with the results from RT-PCR experiments, the expression levels of SR-A increased in a time-dependent manner after hyperoxia treatment. Representative data from two independent experiments are shown

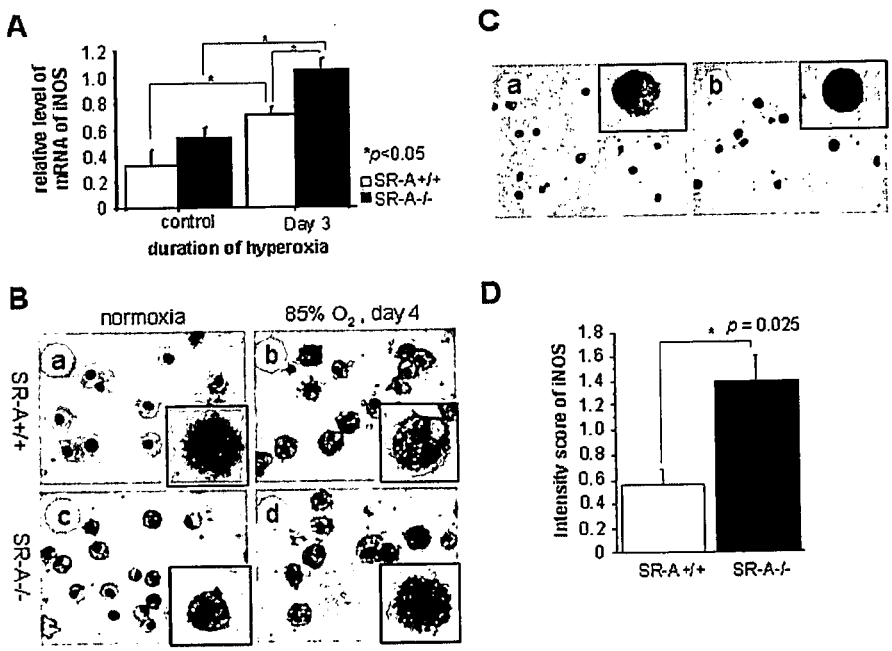

Figure 4. (A) Levels of iNOS mRNA in lung tissues determined by real-time RT-PCR. A significant increase of iNOS mRNA was observed at day 3 compared with day 0 in both groups. The level of iNOS mRNA at day 3 in SR-A$^{-/-}$ mice was significantly increased compared with SR-A$^{+/+}$ mice. Lung tissue from four mice in each group at each time point was used. (B) Immunocytochemistry of iNOS in alveolar macrophages. Alveolar macrophages collected from BALF from SR-A$^{+/+}$ mice (a, b) or SR-A$^{-/-}$ mice (c, d) at day 0 (a, c) or at day 4 (b, d) after exposure to 85% O_2. Macrophages from SR-A$^{-/-}$ mice expressed intense immunoreactivity against iNOS after hyperoxia (d) compared with that from SR-A$^{+/+}$ mice (b). Original magnification ×400. (C) Immunocytochemical expression of iNOS in cultured alveolar macrophages. Alveolar macrophages collected from SR-A$^{+/+}$ (a) and SR-A$^{-/-}$ mice (b) were cultured in a hyperoxic tissue culture incubator for 72 h. The intensity of iNOS staining is stronger in SR-A$^{-/-}$ macrophages than in SR-A$^{+/+}$ macrophages. Original magnification ×200. (D) Comparison of the iNOS staining intensity between SR-A$^{+/+}$ (open bar) and SR-A$^{-/-}$ (solid bar) alveolar macrophages after hyperoxic treatment *in vitro* for 72 h. The mean iNOS score was 0.56 ± 0.12 in SR-A$^{+/+}$ macrophages and 1.40 ± 0.20 in SR-A$^{-/-}$ macrophages. The difference is statistically significant ($p = 0.025$). Values are expressed as means ± SEM; three mice were studied from each group

J Pathol 2007; **212**: 38–46 DOI: 10.1002/path

macrophages to 85% O_2 for 72 h also showed similar results (Figure 4C). Semi-quantitative evaluation revealed that the intensity of staining for iNOS was significantly greater in SR-$A^{-/-}$ macrophages than in SR-$A^{+/+}$ macrophages (Figure 4D).

To evaluate the degree of oxidative stress of the lung after hyperoxic exposure, immunostaining with nitrotyrosine was performed. Nitrotyrosine correlates with peroxynitrite-mediated oxidative stress [26]. The intensity of nitrotyrosine immunostaining at day 4 of hyperoxia was greater in samples from SR-$A^{-/-}$ mice than in those from SR-$A^{+/+}$ mice (Figure 5). Sections from both groups of mice in normoxia did not show significant immunohistochemical staining for nitrotyrosine (Figure 5).

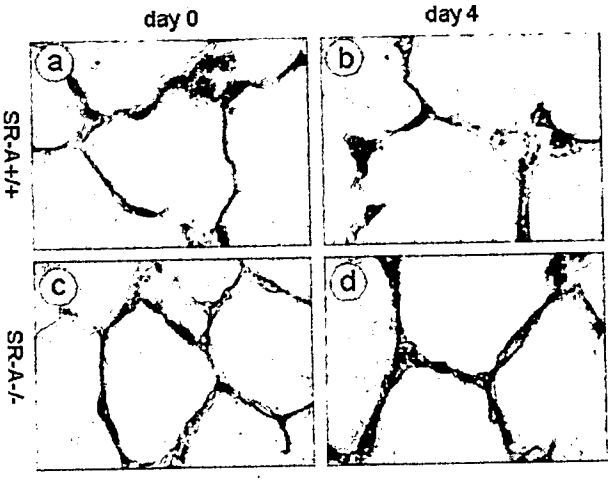

Figure 5. Immunohistochemical staining of nitrotyrosine in lung tissue from SR-$A^{+/+}$ (a, b) and SR-$A^{-/-}$ mice (c, d). No distinct immunostaining was observed at day 0 in either group of mice (a, c). However, at day 4 after hyperoxia treatment (b, d), strong staining of nitrotyrosine was observed in SR-$A^{-/-}$ mice (d). Nitrotyrosine labelling is seen at the alveolar wall, presumably in alveolar epithelial cells. Original magnification ×1000

TNF-α expression

TNF-α is a representative inflammatory cytokine involved in various pathological processes and it is well known to accelerate oxidative stress during inflammation [27,28]. To demonstrate the mechanism by which SR-A alters oxidative stress during hyperoxic lung injury, we assessed the levels of TNF-α mRNA in lungs with hyperoxic injury. Although the mRNA levels of TNF-α increased in a time-dependent manner in both phenotypes, the levels in SR-$A^{-/-}$ mice at day 1 were significantly higher than those in SR-$A^{+/+}$ mice. In addition, the TNF-α mRNA levels reached a plateau earlier in SR-$A^{-/-}$ mice than in SR-$A^{+/+}$ mice (Figures 6A and 6B).

Discussion

Hyperoxia activates alveolar macrophages to release reactive oxygen species as well as pro-inflammatory cytokines. Although the mechanisms of hyperoxia-induced acute lung injury are very complicated, the role of alveolar macrophages has been highlighted, particularly as a source of huge amounts of nitric

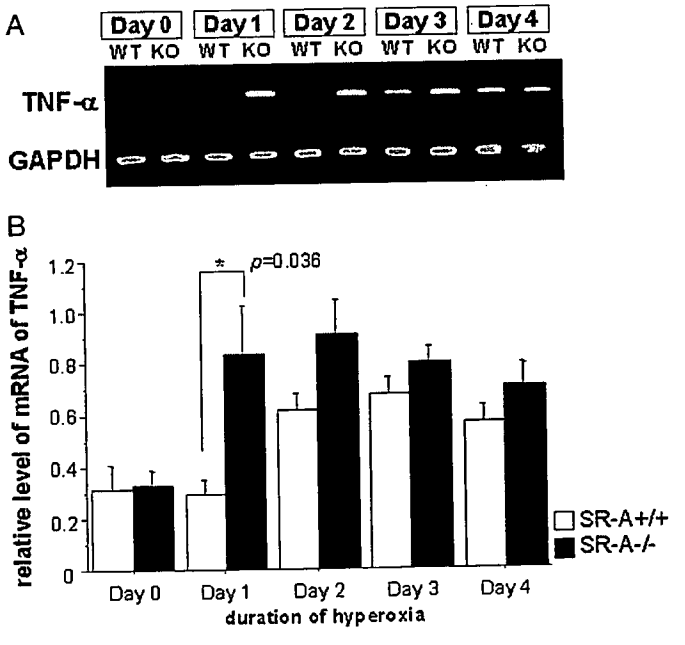

Figure 6. Levels of TNF-α mRNA in lungs with or without 85% O_2 treatment. Total RNA was extracted from tissue samples and subjected to RT-PCR with primers specific for TNF-α and GAPDH as outlined in the text. (A) Representative amplified RT-PCR products after gel electrophoresis. (B) Semi-quantitative demonstration of levels of TNF-α before and after hyperoxic treatment of both SR-A phenotypes. Data are presented as ratios of the densitometric values of TNF-α to GAPDH. Signals of TNF-α mRNA were increased after induction of hyperoxia in both phenotypes. TNF-α signals in SR-$A^{-/-}$ mice increased rapidly and reached a plateau compared with wild-type mice. Tissue from four mice per group at each time point was used

oxide [10]. In the present study, we have clearly shown that SR-A$^{-/-}$ mice are more susceptible to hyperoxia-induced lung injury than SR-A$^{+/+}$ mice. Higher protein levels in BALF and the increased ratio of wet to dry lung weight of hyperoxia-treated SR-A$^{-/-}$ mice indicate that hyperoxic damage to alveolar epithelium and vascular endothelium and the resultant severe pulmonary oedema are greatly increased in SR-A$^{-/-}$ mice. Hyperoxia induced increases in iNOS mRNA and protein levels in both groups of mice; however, the increases in SR-A$^{-/-}$ mice were significantly greater. The level of oxidative stress estimated by the formation of nitrotyrosine was stronger in SR-A$^{-/-}$ mice than in SR-A$^{+/+}$ mice.

It is widely accepted that the key event of hyperoxic lung injury is oxidative stress, especially with regard to the oxidation of pneumocytes [25]. This process is mediated by peroxynitrite anions, which are derived from a direct reaction between superoxide anions and nitric oxide. Previous reports have demonstrated that an excessive amount of nitric oxide is toxic to lung tissue [29]. Explosive nitric oxide production by iNOS in various types of activated cells suggests that iNOS is likely to be localized to specific sites of nitric oxide production and action. Many inflammatory stimuli including hyperoxia increase the expression of iNOS in endothelial cells, epithelial cells, neutrophils, and macrophages [10,30–32]. During hyperoxia-mediated alveolar damage, alveolar macrophages are believed to be a major source of nitric oxide derived from iNOS [33]. The nitric oxide metabolite, peroxynitrite, may react with tyrosine residues of various proteins to form nitrotyrosine [34]. Nitrotyrosine is a relatively specific marker for the formation of peroxynitrite, and increased levels of nitrotyrosine reflect increased levels of oxidative stress [10,35]. Strong nitrotyrosine staining in SR-A$^{-/-}$ mice (Figure 5) is indicative of augmented oxidative stress and consequent alveolar damage.

It is noteworthy that the SR-A expression in alveolar macrophages from wild-type mice was augmented during the course of hyperoxic treatment. It is likely that such increases of SR-A are protective against lung damage, since SR-A will scavenge any newly produced harmful oxidized materials. Oxidative stress-related increases in iNOS expression during hyperoxic lung injury are mediated by pro-inflammatory cytokines. Previous reports have demonstrated that hyperoxia induces a wide variety of pro-inflammatory cytokines such as TNF-α and IL-6 [36]. Consistent with our data, an increase in the TNF-α levels in the injured lung is one of the earliest cellular responses to hyperoxia [5,37]. TNF-α induces increased iNOS expression in the lung [38]. Increased expression of TNF-α in SR-A$^{-/-}$ mice exacerbates hyperoxic lung injury. Pretreatment of animals with anti-TNF-α antibody attenuates hyperoxia-induced lung injury, indicating that TNF-α plays a critical role in hyperoxic lung injury [38]. Hence, higher levels of TNF-α expression in SR-A$^{-/-}$ mice may cause increased production of iNOS and extended oxidative stress in this phenotype.

Macrophage counts in BALF were not different between SR-A$^{+/+}$ and SR-A$^{-/-}$ mice in our model, consistent with the other model by Beamer and Holian [20]. They reported that the number of macrophages did not change in the silica-induced lung injury model, in spite of the higher TNF-α level in BALF of SR-A$^{-/-}$ mice. Future evaluation of chemokines and other cytokines will delineate this process.

SR-A is a multifunctional molecule expressed in macrophages. Recently, the repertoire of SR-A functions has been extended; several studies have demonstrated that SR-A regulates the cytokine production, such as TNF-α, IL-6, and IL-12, in response to various kinds of inflammatory stimuli [18–20,39,40]. Haworth *et al* reported that SR-A$^{-/-}$ mice produce TNF-α and IL-6 in response to LPS and are susceptible to endotoxin [19]. In addition, Ozeki *et al* found that SR-A$^{-/-}$ alveolar macrophages treated with mycobacterium cord factor secreted larger amounts of TNF-α compared with wild-type controls, and treatment of SR-A$^{+/+}$ macrophages with anti-SR-A antibodies increased TNF-α production [18]. Moreover, Beamer Holian discovered that TNF-α levels in BALF after silica inhalation were significantly increased in SR-A$^{-/-}$ compared with SR-A$^{+/+}$ mice [20]. LPS, mycobacterial cord factor, and silica are considered to be ligands of SR-A [41]. This suggests that ligand-bound SR-A may suppress inflammatory responses by reducing TNF-α production. Although the nature of ligand(s) for SR-A in the present study is not clear, we assume that oxidized materials in the alveolar space may bind SR-A.

Activation of transcription factors such as nuclear factor-κB (NF-κB) and activator protein-1 (AP-1) has been reported to be involved in hyperoxia-induced organ injury [42,43]. Further studies inducing various levels of NF-κB and AP-1 in hyperoxia-induced lung injury models will help to elucidate the mechanisms involved in SR-A regulation of inflammatory response and oxidative stress.

In summary, we report that hyperoxia increases SR-A expression in murine lungs. SR-A$^{-/-}$ mice were more susceptible to hyperoxic lung injury, with increased levels of TNF-α and iNOS producing more severe oxidative stress in this SR-A$^{-/-}$ phenotype. Taken together, these data suggest that intrapulmonary SR-A expression reduces macrophage activation and protects against acute alveolar injury such as hyperoxic lung damage.

Acknowledgements

We thank Mr Takenobu Nakagawa, Mr Osamu Nakamura, Ms Emi Kiyota, and Mr Junichi Yoshida for their technical assistance, and Ms Junko Imura for the secretarial effort. This study was supported in part by Grants-in-Aid for Scientific Research (B16390108, C17590797) from the Ministry of Education, Culture, Sports, Science, and Technology of Japan.

Supplementary material

Supplementary material may be found at the web address http://www.interscience.wiley.com/jpages/0022-3417/suppmat/path.2150.html.

References

1. Toyokuni S. Reactive oxygen species-induced molecular damage and its application in pathology. *Pathol Int* 1999;**49:**91–102.
2. Frank L, Bucher JR, Roberts RJ. Oxygen toxicity in neonatal and adult animals of various species. *J Appl Physiol* 1978;**45:**699.
3. Fischer AB, Forman HJ, Glass M. Mechanisms of pulmonary oxygen toxicity. *Lung* 1984;**162:**255–259.
4. Chabot F, Mitchell JA, Gutteridge JM, Evans TW. Reactive oxygen species in acute lung injury. *Eur Respir J* 1998;**11:**745–757.
5. Guthmann F, Wissel H, Schachtrup C, Tolle A, Rudiger M, Spener F, *et al.* Inhibition of TNF-alpha *in vivo* prevents hyperoxia-mediated activation of caspase 3 in type II cells. *Respir Res* 2005;**6:**10.
6. Lindsay L, Oliver SJ, Freeman SL, Josien R, Krauss A, Kaplan G. Modulation of hyperoxia-induced TNF-alpha expression in the newborn rat lung by thalidomide and dexamethasone. *Inflammation* 2000;**24:**347–356.
7. Tsan MF, White JE, Michelsen PB, Wong GH. Pulmonary O_2 toxicity: role of endogenous tumor necrosis factor. *Exp Lung Res* 1995;**21:**589–597.
8. Worrall NK, Chang K, LeJeune WS, Misko TP, Sullivan PM, Ferguson TB Jr, *et al.* TNF-alpha causes reversible *in vivo* systemic vascular barrier dysfunction via NO-dependent and -independent mechanisms. *Am J Physiol* 1997;**273:**2565–2574.
9. Kobayashi H, Hataishi R, Mitsufuji H, Tanaka M, Jacobson M, Tomita T, *et al.* Antiinflammatory properties of inducible nitric oxide synthase in acute hyperoxic lung injury. *Am J Respir Cell Mol Biol* 2001;**24:**390–397.
10. Hesse AK, Dorger M, Kupatt C, Krombach F. Proinflammatory role of inducible nitric oxide synthase in acute hyperoxic lung injury. *Respir Res* 2004;**5:**11.
11. Haddad IY, Pataki G, Hu P, Galliani C, Beckman JS, Matalon S. Quantitation of nitrotyrosine levels in lung sections of patients and animals with acute lung injury. *J Clin Invest* 1994;**94:**2407–2413.
12. Suzuki H, Kurihara Y, Takeya M, Kamada N, Kataoka M, Jishage K, *et al.* A role for macrophage scavenger receptors in atherosclerosis and susceptibility to infection. *Nature* 1997;**386:**292–296.
13. Suzuki H, Kurihara Y, Takeya M, Kamada N, Kataoka M, Jishage K, *et al.* The multiple roles of macrophage scavenger receptors (MSR) *in vivo*: resistance to atherosclerosis and susceptibility to infection in MSR knockout mice. *J Atheroscler Thromb* 1997;**4:**1–11.
14. Sakaguchi H, Takeya M, Suzuki H, Hakamata H, Kodama T, Horiuchi S, *et al.* Role of macrophage scavenger receptors in diet-induced atherosclerosis in mice. *Lab Invest* 1998;**78:**423–434.
15. Krieger M, Acton S, Ashkenas J, Person A, Penman M, Resnick D. Molecular flypaper, host defense, and atherosclerosis. *J Biol Chem* 1993;**268:**4569–4572.
16. Mori T, Takahashi K, Higashi T, Takeya M, Kume S, Kawabe Y, *et al.* Localization of advanced glycation end products of Millard reaction in bovine tissues and their endocytosis by macrophage scavenger receptors. *Exp Mol Pathol* 1995;**63:**135–152.
17. Platt N, Haworth R, Darley L, Gordon S. The many roles of the class A macrophage scavenger receptor. *Int Rev Cytol* 2002;**212:**1–40.
18. Ozeki Y, Tsutsui H, Kawada N, Suzuki H, Kataoka M, Kodama T, *et al.* Macrophage scavenger receptor down-regulates mycobacterial cord factor-induced proinflammatory cytokine production by alveolar and hepatic macrophages. *Microb Pathog* 2006;**40:**171–176.
19. Haworth R, Platt N, Keshav S, Hughes D, Darley E, Suzuki H, *et al.* The macrophage scavenger receptor type A is expressed by activated macrophages and protects the host against lethal endotoxic shock. *J Exp Med* 1997;**186:**1431–1439.
20. Beamer CA, Holian A. Scavenger receptor class A type I/II (CD204) null mice fail to develop fibrosis following silica exposure. *Am J Physiol Lung Cell Mol Physiol* 2005;**289:**186–195.
21. Okuma T, Terasaki Y, Sakashita N, Kaikita K, Kobayashi H, Hayasaki T, *et al.* MCP-1/CCR2 signaling is involved in hyperoxia-induced acute lung injury by regulating nitric oxide production. *Int J Exp Pathol* 2006;**87:**475–483.
22. Okuma T, Terasaki Y, Kaikita K, Kobayashi H, Kuziel WA, Kawasuji M, *et al.* C–C chemokine receptor 2 (CCR2) deficiency improves bleomycin-induced pulmonary fibrosis by attenuation of both macrophage infiltration and production of macrophage-derived matrix metalloproteinases. *J Pathol* 2004;**204:**594–604.
23. Tomokiyo R, Jinnouchi K, Honda M, Wada Y, Hanada N, Hiraoka T, *et al.* Production, characterization, and inter-species reactivities of monoclonal antibodies against human class A macrophage scavenger receptors. *Atherosclerosis* 2002;**161:**123–132.
24. Crapo JD, Barry BE, Foscue HA, Shelburne J. Structural and biochemical changes in rat lungs occurring during exposures to lethal and adaptative doses of oxygen. *Am Rev Respir Dis* 1980;**122:**123–143.
25. Narasaraju TA, Jin N, Narendranath CR, Chen Z, Gou D, Liu L. Protein nitration in rat lungs during hyperoxia exposure: a possible role of myeloperoxidase. *Am J Physiol Lung Cell Mol Physiol* 2003;**285:**1037–1045.
26. Haddad IY, Pataki G, Hu P, Galliani C, Beckman JS, Matalon S. Quantitation of nitrotyrosine levels in lung sections of patients and animals with acute lung injury. *J Clin Invest* 1994;**94:**2407–2413.
27. Glosli H, Tronstad KJ, Wergedal H, Muller F, Svardal A, Aukrust P, *et al.* Human TNF-alpha in transgenic mice induces differential changes in redox status and glutathione-regulating enzymes. *FASEB J* 2002;**16:**1450–1452.
28. Brown LA, Harris FL, Guidot DM. Chronic ethanol ingestion potentiates TNF-alpha-mediated oxidative stress and apoptosis in rat type II cells. *Am J Physiol Lung Cell Mol Physiol* 2001;**281:**377–386.
29. Rossaint R, Falke KJ, Lopez F, Slama K, Pison U, Zapol WM. Inhaled nitric oxide for the adult respiratory distress syndrome. *N Engl J Med* 1993;**328:**399–405.
30. Schulz C, Gillissen A, Schultze-Werninghaus G. Inducible nitric oxide synthase in pulmonary inflammatory processes. *Pneumologie* 1998;**52:**340–349.
31. Hickey MJ, Sharkey KA, Sihota EG, Reinhardt PH, Macmicking JD, Nathan C, *et al.* Inducible nitric oxide synthase-deficient mice have enhanced leukocyte–endothelium interactions in endotoxemia. *FASEB J* 1997;**11:**955–964.
32. Ermert M, Ruppert C, Gunther A, Duncker HR, Seeger W, Ermert L. Cell-specific nitric oxide synthase-isoenzyme expression and regulation in response to endotoxin in intact rat lungs. *Lab Invest* 2002;**82:**425–441.
33. Mehta S. The effects of nitric oxide in acute lung injury. *Vascul Pharmacol* 2005;**43:**390–403.
34. Beckmann JS, Ye YZ, Anderson PG, Chen J, Accavitti MA, Tarpey MM, *et al.* Extensive nitration of protein tyrosines in human atherosclerosis detected by immunohistochemistry. *Biol Chem Hoppe Seyler* 1994;**375:**81–88.
35. Eiselich JP, Hristova M, Cross CE, Jones AD, Freeman BA, Hailliwell B, *et al.* Formation of nitric oxide-derived inflammatory oxidants by myeloperoxidase in neutrophils. *Nature* 1998;**391:**393–397.
36. Ben-Ari J, Makhoul IR, Dorio RJ, Buckley S, Warburton D, Walker SM. Cytokine response during hyperoxia: sequential production of pulmonary tumor necrosis factor and interleukin-6 in neonatal rats. *Isr Med Assoc J* 2000;**2:**365–369.
37. Desmarquest P, Chadelat K, Corroyer S, Cazals V, Clement A. Effect of hyperoxia on human macrophage cytokine response. *Respir Med* 1998;**92:**951–960.
38. Wherry JC, Pennington JE, Wenzel RP. Tumor necrosis factor and the therapeutic potential of anti-tumor necrosis factor antibodies. *Crit Care Med* 1993;**21:**436–440.

39. Coller SP, Paulnock DM. Signaling pathways initiated in macrophages after engagement of type A scavenger receptors. *J Leukoc Biol* 2001;**70:**142–148.
40. Jozefowski S, Kobzik L. Scavenger receptor A mediates H_2O_2 production and suppression of IL-12 release in murine macrophages. *J Leukoc Biol* 2004;**76:**1066–1074.
41. Platt N, Gordon S. Is the class A macrophage scavenger receptor (SR-A) multifunctional? — The mouse's tale. *J. Clin Invest* 2001;**108:**649–654.
42. Lee PJ, Choi AM. Pathways of cell signaling in hyperoxia. *Free Radic Biol Med* 2003;**35:**341–350.
43. Pepperl S, Dorger M, Ringel F, Kupatt C, Krombach F. Hyperoxia upregulates the NO pathway in alveolar macrophages *in vitro*: role of AP-1 and NF-kappaB. *Am J Physiol Lung Cell Mol Physiol* 2001;**280:**905–913.

Microscopic-Sized "Microthymoma" in Patients With Myasthenia Gravis*

Takeshi Mori, MD; Hiroaki Nomori, MD, PhD; Koei Ikeda, MD, PhD; Hironori Kobayashi, MD; Kazunori Iwatani, MD; Masakazu Yoshioka, MD; and Ken-ichi Iyama, MD, PhD

Background: **In 2005, Cheuk et al reported two patients with microscopic-sized thymomas and proposed the term *microthymoma* to distinguish it from the nodular hyperplasia of thymic epithelium, so-called *microscopic thymoma*. Here, we present microthymomas that were found in 196 patients with myasthenia gravis (MG) who had undergone thymectomy.**

Materials and methods: **Thymic tissues in 196 patients with MG who underwent thymectomy or thymothymomectomy were examined. Of these patients, 73 patients had thymoma indicated by CT before surgery, and the other 123 patients had no mediastinal tumors. From the resected thymic tissues, an average of 14 hematoxylin-eosin–stained sections (range, 4 to 55 sections) were prepared for microscopic examination. The histologic type of the thymoma was classified according to the World Health Organization (WHO) classification.**

Results: **From the 196 patients, we found three microthymomas in 3 patients (1.5%). While these three tumors could not be seen grossly in pathology section, they were found microscopically (range, 2 to 4 mm). The histologic subtype according to the WHO classification system was B1 in one patient and B2 in two patients.**

Conclusion: **Microthymoma was found in 3 of 196 patients (1.5%) with MG. Microthymoma might exist in thymus of patients with MG, even in patients who have no thymoma indicated by CT.**

(CHEST 2007; 131:847–849)

Key words: microthymoma; myasthenia gravis; thymectomy; thymoma

Abbreviations: HE = hematoxylin-eosin; MG = myasthenia gravis; WHO = World Health Organization

In 2005, Cheuk et al[1] reported two cases of microscopic-sized thymoma. They proposed calling such small thymomas *microthymoma* to distinguish them from the microscopic thymoma, which is composed of small thymic epithelial nests, and it has been suggested that a more appropriate term would be *nodular hyperplasia* of the thymic epithelium.[2] In this report, we discuss three patients with microthymoma from a population of 196 patients with myasthenia gravis (MG) who had undergone thymectomy or thymothymomectomy. We also review another four case reports of microthymoma from the English-language literature.

The ethical committee of Kumamoto University Hospital approved this retrospective study of patients with MG in March 2006. From November 1985 to February 2006, 196 patients with MG underwent thymectomy or thymothymomectomy in the Department of Thoracic Surgery at Kumamoto University Hospital. Of these, 73 patients had thymoma indicated by CT before surgery, and the other 123 patients had no mediastinal tumors. From the resected thymic tissue, an average of 14 hematoxylin-

*From the Department of Thoracic Surgery (Drs. Mori, Nomori, Ikeda, Kobayashi, Iwatani, and Yoshioka), Graduate School of Medical Sciences, and Department of Surgical Pathology (Dr. Iyama), Kumamoto University Hospital, 1–1-1 Honjo, Kumamoto 860-8556, Japan.

The authors have no conflicts of interest to disclose.

Manuscript received August 12, 2006; revision accepted October 2, 2006.

Correspondence to: Hiroaki Nomori, MD, PhD, Department of Thoracic Surgery, Graduate School of Medical Sciences, Kumamoto University, 1–1-1 Honjo, Kumamoto 860-8556, Japan; e-mail: hnomori@qk9.so-net.ne.jp

DOI: 10.1378/chest.06-2014